Numerical solution of the Schrödinger equation using discrete kinetic theory

Sauro Succi
Istituto Applicazioni del Calcolo, V. le Policlinico 137, 00161 Roma, Italy
(Received 7 August 1995)

The quantum lattice Boltzmann equation a new variant of the lattice Boltzmann equation specifically designed to describe quantum mechanical motion, is checked against analytical results for the case of a free particle and the harmonic oscillator in (1+1) space-time dimensions. The proper parameter regime under which the method needs to be operated in order to reproduce faithfully nonrelativistic quantum motion is discussed.

PACS number(s): 02.70.−c, 03.65.−w

I. INTRODUCTION

The Dirac equation is the most general equation describing single particle motion in compliance with the two fundamental pillars of modern physics: quantum theory and special relativity. Relativistic effects are controlled by the ratio of particle to light speed $\beta=v/c$, while quantum effects are driven by nonvanishing values of the (imaginary) diffusion coefficient $\hbar/2m$, m being the particle rest mass [1]. In a recent paper, a procedure to solve quantum mechanical problems using numerical techniques mutuated from discrete kinetic theory has been proposed [2]. This procedure builds on a formal analogy between the Dirac equation and a special discrete kinetic equation known as the lattice Boltzmann equation (LBE). In particular, it was shown that by a proper resort to operator splitting methods, the Dirac equation can be integrated as a sequence of three one-dimensional LBE's evolving complex-valued distribution functions.

It is the purpose of this paper to investigate the ability of the numerical procedure outlined in Ref. [2] to properly describe the nonrelativistic quantum motion starting from a relativistic equation such as the Quantum LBE (QLBE).

The method should in principle be able to follow relativistic motion as well, but a quantitative assessment along this direction would require a separate study in its own. As a result, in this paper we shall restrict ourselves to nonrelativistic quantum motion as described by the Schrödinger equation.

II. QUANTUM LBE

For the sake of simplicity, we shall confine our discussion to one-dimensional motion (1+1) of a free quantum relativistic particle. Using the Majorana representation [3], and projecting upon chiral eigenstates, the Dirac equation reads as follows:

$$\begin{aligned} \partial_t d - c\partial_z d &= -\omega_c u + igd \ , \\ \partial_t u + c\partial_z u &= +\omega_c d + igu \ , \end{aligned} \tag{1}$$

where u and d represent a pair of complex bispinors, $\omega_c=mc^2/\hbar$ is the Compton frequency, and $g=qV/\hbar$ is the (space-dependent) frequency coupling to the external potential V, q being the particle electric charge. Since we confine our attention to electrostatic potentials, the spinorial indices will be dropped throughout the paper.

As noted in [1], Eq. (1) can be interpreted as a discrete Boltzmann equation for a pair of complex distribution wave functions u and d, streaming along the z axis with opposite speeds $\pm c$, and undergoing collisions according to the scattering matrix defined by the right-hand side of Eq. (1).

In the collisionless limit ($m\to 0, g\to 0$), Eq. (1) describes two light pulses propagating undisturbed and passing transparently across one another as befits photonic wave functions. This is the fully hyperbolic, relativistic regime described by the Klein-Gordon equation for spinless bosons.

Once a material mass is switched on, the two photonic pulses start to interact so as to produce drag (a particle speed slower than light speed) and diffusion (a loss of quantum coherence) on the distribution functions.

Nonrelativistic motion emerges in the adiabatic (low-frequency) limit:

$$\omega \ll |\omega_c + g| \ . \tag{2}$$

With the further constraint of "small" potential coupling

$$|g| \ll \omega_c \ , \tag{3}$$

it is readily checked that the slow mode [see Eq. (11)] dynamics is governed by the Schrödinger equation for a spinless particle of mass m.

It is worth noting that, in this "kinetic-theory-inspired" view, both quantum and relativistic effects can be traced back to a simple common kinetic origin: a nonzero particle collision frequency.

This is somehow suggestive of a "hidden-variables" theory, whereby the wave function plays the role of a coarse-grained variable resulting from the collective motion of a cloud of unobservable "automata" all propagating synchronously in lock-step mode at light speed, and undergoing collisions according to the right-hand side of Eq. (1). Leaving aside this controversial subject, we turn to the issue of numerical discretization.

According to the procedure prosed in [2], the system of equations (1) is discretized via a Cranc-Nicolson time-marching scheme combined with a (somewhat unconventional) upwind treatment of the spatial derivatives. This means that the space derivatives are replaced by one-sided discrete differences taken along the streaming direction, i.e., forward differences for upward propagating modes and backward differences for the downward-moving modes.

By working in atomic units ($c=\hbar=q=1$) and normalizing space time in units of lattice spacings ($\Delta x=\Delta t=1$), we are led to the following set of algebraic equations:

$$\begin{aligned} \hat{u}-u &= au+bd \ , \\ \hat{d}-d &= ad-bu \ , \end{aligned} \tag{4}$$

where $u=u(z,t)$, $d=d(z,t)$ and $\hat{d}=d(z-1,t+1)$, $\hat{u}=u(z+1,t+1)$. The scattering elements are given by

$$\begin{aligned} a &= (1-\Omega/4)/(1-\Omega/4+ig) \ , \\ b &= m/(1-\Omega/4+ig) \ , \end{aligned} \tag{5}$$

where $\Omega=m^2-g^2$, $u=u(z,t)$, and $d=d(z,t)$, and m represents the dimensionless Compton frequency in lattice units ($\Delta x=\Delta t=c=q=1$).

Equation (4) preserves unitarity (norm conservation) all along the time evolution under the condition

$$a^2+b^2=1 \ . \tag{6}$$

It is readily checked that the scattering matrix defined by Eqs. (4) and (5) does indeed comply with the above conservation law. In addition, owing to the upwind treatment of the spatial variable, the scheme is also unconditionally stable and dispersion free. Another remarkable feature due to the upwind scheme is that unconditional stability can be obtained without spoiling the matrix freedom of the numerical scheme. This is due to the fact that the linear system generated by the implicit Cranc-Nicolson time-stepping procedure is easily solved algebraically site by site to yield expressions (4) with no need to introduce any matrix solver.

III. NUMERICAL TEST 1: FREE PROPAGATION

Free-particle dynamics is recovered from Eq. (1) by simply letting the coupling constant $g\to 0$. This test is trivial from the physical point of view, but is well suited to isolate numerical issues from the physical ones.

The nonrelativistic limit is most conveniently discussed by inspecting the dispersion relation associated with Eq. (4). This reads

$$\omega_{\pm}=\pm\sqrt{k^2+m'^2} \ , \tag{7}$$

where $m'=\arctan[m/(1-m^2/2)]$ is an effective mass incorporating the effects of lattice discreteness. In the limit $m\to 0$, m' reduces to m as imposed by consistency requirements. This sets an upper bound to m which is, however, rather soft because, due to the shape of the arctan function, m' remains close to m except for $m\simeq 1$. As a result, in the following we shall always refer to m, with the tacit assumption $m<1$.

The Schrödinger equation follows from the Dirac equation in the limit of long wavelength and low frequencies:

$$k^2 \ll m^2 \ , \tag{8}$$

or, equivalently, in our units,

$$\beta=k/m \ll 1 \ . \tag{9}$$

In order to test the validity of our scheme in this regime, we evolve the following pair of minimum uncertainty wave packets:

$$\Psi_{u,d}=(2\pi T_0)^{-1/4}\exp\left[-\frac{(z-z_0)^2}{4T_0}\right] \times\exp[\pm i\beta_0(z-z_0/2)] \ . \tag{10}$$

This expression represents two wave packets centered about z_0, with an initial spread $\Delta_0=\sqrt{T_0}$ propagating at speed β_0 along the $+z$ (particle) and $-z$ (antiparticle) axes, respectively.

Following a standard procedure, we introduce a pair of transformed wave functions defined as follows:

$$\phi_{\pm}=\frac{1}{\sqrt{2}}(u\pm id)\exp(-imt) \ , \tag{11}$$

which represent the slow (+) hydrodynamic and fast (−) nonhydrodynamic modes, respectively. Note that these modes combine a weighted mix of particle (u) and antiparticle (d) states.

It is a simple matter to show that the fast mode amplitude is of order $O(\beta)$ with respect to the hydrodynamic mode, and its oscillation frequency is $O(\beta^{-1})$. As a result, in the adiabatic limit $\beta\to 0$, the fast mode decouples from the system dynamics which is consequently dominated by the slow mode. It is precisely under these conditions that nonrelativistic quantum motion is expected to emerge out of the Dirac equation (1).

To check the ability of QLBE to reproduce this dynamical decoupling, we monitored the main representative parameters associated with the wave motion, i.e., the mean displacement $Z=\langle z\rangle$ and the mean spread $\Delta=(\langle z-Z\rangle^2)^{1/2}$.

As is well known [4], these quantities evolve accordingly to the following exact equation:

$$Z(t)=z_0+\beta t \tag{12}$$

and

$$\Delta(t)=\left[\Delta_0^2+\frac{t^2}{4m^2\Delta_0^2}\right]^{1/2} \ . \tag{13}$$

In Fig. 1 we show $Z-z_0$ and Δ as a function of time for the following choice of parameters: $m=0.1$, $\Delta_0=50$, and $z_0=1024$, on a 2048-point mesh.

The suffix (+) denotes averaging over $\rho_+=|\phi_+^2|$. From this figure, one can appreciate a remarkable match of the (+) quantities with the analytical results [the short solid segments indicate the analytical slope derived from Eqs. (12) and (13) in the limit $t\gg 1$].

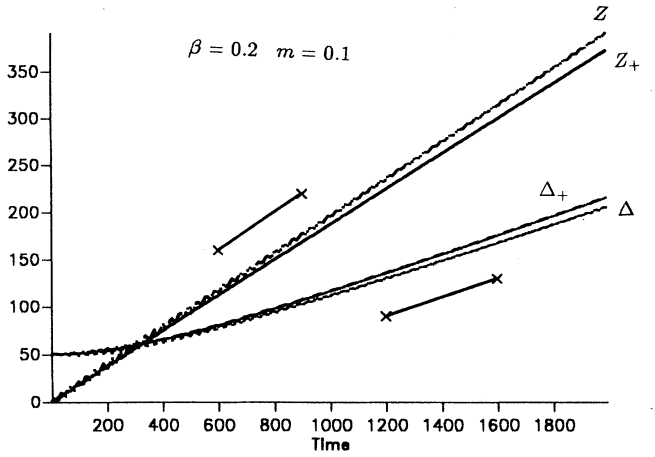

FIG. 1. Mean displacement and variance of the wave function as a function of time for $\beta_0=0.2$ and $m=0.1$. The suffix (+) indicates the average over the density of the hydrodynamic mode.

In Fig. 2 we show the probability distribution function ρ_+ as a function of the space for three different times. A typical drift-diffusion behavior is clearly visible.

A series of runs at different values of β invariably showed that indeed the probability density of the nonhydrodynamic mode is order β^2 with respect to the hydrodynamic one. These results prove that the adiabatic limit of Eq. (1) correctly describes nonrelativistic Schrödinger dynamics.

At this point it is worth mentioning that the quality of the results is affected not only by the value of m but also by the choice of the initial spread Δ_0. This parameter must be kept sufficiently large so as to prevent high wave numbers from violating the adiabaticity conditions Eq. (2).

Note in fact, that the range of wave numbers active during wave motion is approximately given by

$$|k| \sim |k_0 + 2\pi/\Delta(t)| < |k_0 + 2\pi/\Delta_0| \ . \tag{14}$$

This relation shows that adiabaticity can be violated whenever $\Delta_0 < 1/k_0$, even though k_0 lies well within the nonrelativistic range. This inequality is indeed fulfilled for the present simulations ($\Delta_0=50$).

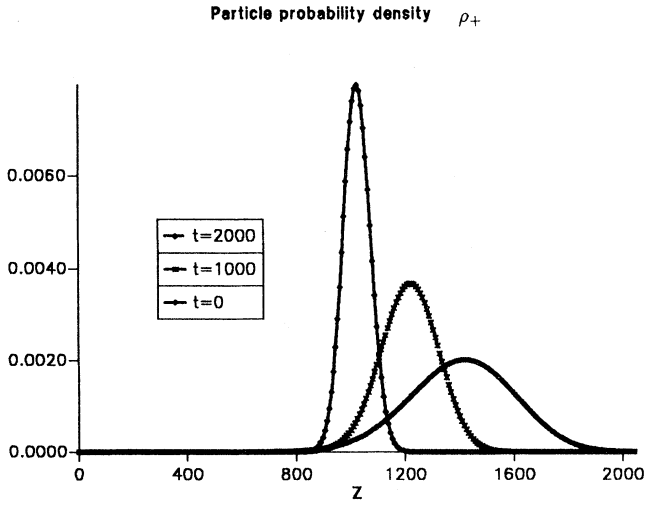

FIG. 2. Probability distribution ρ_+ of the hydrodynamic mode at three different times $t=0$, 1000, 2000 for the same parameters as Fig. 1. A typical drift-diffusion behavior is clearly visible.

IV. NUMERICAL TEST 2: HARMONIC OSCILLATOR

As a second test, we consider a one-dimensional harmonic oscillator, namely a quantum particle trapped within a parabolic potential centered about the midpoint of the computational domain and attaining its maximum V_0 at the edges $z=0$ and L.

$$V(z)=V_0\left[\frac{z-L/2}{L/2}\right]^2 . \tag{15}$$

It is well known that, for such a potential, time-dependent exact solutions exist in the form of coherent wave packets:

$$\Phi_{\rm wp}=(2\pi\Delta^2)^{-1/4}\exp\left[-\frac{[z-Z(t)]^2}{4\pi\Delta^2}\right]\exp -iP(t)\exp\left[-\frac{i\omega_0 t}{2}\right] , \tag{16}$$

where the mean quantities $Z(t)$ and $P(t)$ obey the classical equations of motion of the harmonic oscillator:

$$\dot{Z}=P/m \ , \tag{17}$$

$$\ddot{Z}+\omega_0^2 Z=0 \ , \tag{18}$$

where

$$\omega_0^2=1/2m\Delta_0^2 . \tag{19}$$

Remarkably enough, these wave packets do not disperse because quantum diffusion is exactly counterbalanced by the linear force associated with the harmonic potential. In particular, the spreading Δ_0 characterizes the ground state of the harmonic oscillator and is therefore exactly preserved all along the evolution. This is true only in the nonrelativistic limit.

We have checked the ability of QLBE to preserve quantum coherence over an extensive series of runs by varying the parameters V_0, m, and L so as to produce the following sequence of spreadings: $\Delta_0=64$, 32, and 16.

A series of results is reported in Table I. Here Δ is the wave-function variance averaged over 3–6 periods. From this table, we observe that good agreement is obtained on the smaller grids. The deterioration on larger

TABLE I. Loss of coherence as a function of the grid size for case A ($\Delta_0=64$). The theoretical spreading is 64 lattice units.

L	V_0	m	Δ
1024	$\frac{1}{32}$	$\frac{1}{16}$	66.1±1.1
2048	$\frac{1}{16}$	$\frac{1}{8}$	67.4±3.1
4096	$\frac{1}{8}$	$\frac{1}{4}$	72.1±4.1

TABLE II. Loss of cohernece as a function of the grid size for case B ($\Delta_0=32$). The theoretical spreading is 32 lattice units.

L	Δ	V_0	m
1024	33.5±1.0	$\frac{1}{8}$	$\frac{1}{4}$
512	33.2±1.1	$\frac{1}{16}$	$\frac{1}{8}$
512	32.6±0.6	$\frac{1}{32}$	$\frac{1}{4}$

grids is mostly due to inaccuracies produced by poorly populated tails in the wave-function profile. In fact, by restricting the integration domain from $(L/4,3L/4)$ the scatter on the variance can be significantly cut down while leaving the mean variance itself essentially unchanged. A different diagnostic, based upon detection of the maximum of the wave-packet density, provides much better results, within a few percent of the theoretical value $1/\sqrt{2\pi}\Delta$.

Narrower packets provide somewhat better results, as indicated in the Tables II and III. Note the slight improvement brought about by the increased separation between m and g ($2m/g$ equals 4 on the second row, and 8 on the third), which, according to inequality (3), helps to recover a better adiabaticity.

All of the above results were obtained at a fixed value of $\beta=0.1$. Higher values of β rapidly show the onset of relativistic motion, especially for narrower packets. This is in line with the fact that—on account of Heisenberg's principle—narrow packets generate high momenta, and hence nonadiabatic motion.

A typical example is illustrated in Table IV. Note that norm conservation is also fulfilled up to a respectable level of accuracy when relativistic motion takes over. This is due to the fact that within this numerical formulation density is locally conserved up to machine accuracy. The average motion is also fairly close to the nonrelativistic trajectory for values of β as high as $\beta\sim0.3$.

Inspection of the wave-function profiles reveals that a significant loss of coherence is already apparent at $\beta=0.2$ even if the variance still appears to be rather close to the theoretical value, and even more so the mean coordinate Z. This suggests that the onset of relativistic motion shows up first on higher order moments, while the average motion is somehow more "resilient" to relativistic corrections. This is again a typical scenario of the hydrodynamic limit of kinetic equations (see Fig. 3). An example of a well-behaved solution at $\beta=0.05$ is shown in Fig. 4.

TABLE III. Loss of coherence as a function of the grid size for case C ($\Delta_0=16$). The theoretical spreading is 16 lattice units.

L	Δ	m	V_0
512	16.9±0.6	$\frac{1}{2}$	$\frac{1}{4}$
256	16.7±0.8	$\frac{1}{4}$	$\frac{1}{8}$
256	16.3±0.5	$\frac{1}{2}$	$\frac{1}{16}$

TABLE IV. Loss of coherence as a function of the particle speed for case A ($\Delta_0=64$). The theoretical spreading is 64 lattice units.

β	Δ	$\delta\rho/\rho$
0.0	66.1±1.1	2.0×10^{-6}
0.2	67.6±3.6	3.3×10^{-5}
0.4	76.1±10.8	1.5×10^{-4}
0.8	156.0±45.9	1.4×10^{-3}

V. NUMERICAL TEST 3: SCATTERING BARRIER

As a third test we shall consider the scattering of a wave packet by a box-shaped repulsive potential. As is well know, the steady-state solution of this problem is given by a superposition of incident, reflected, and transmitted waves with wave numbers k_i, k_r, and k_t, respectively:

$$k_i=k_r=\sqrt{2mE}\ ,\quad k_t=\sqrt{2m(E-V_0)}\ . \tag{20}$$

Manifestly, where the potential exceeds the total energy E, the wave number becomes imaginary, and the transmitted wave undergoes an exponential decay.

The presence of both oscillating and decaying behaviors is apparent from Fig. 5, which illustrates the collision of a coherent wave packet with the potential barrier. The numerical parameters of this simulation are

$$\begin{aligned} &L=16\,384\ ,\quad m=0.2\ ,\quad U_0=0.1\ ,\\ &V_0=0.002\ ,\quad \Delta_0=128\ , \end{aligned} \tag{21}$$

corresponding to the wavelengths

$$\lambda_{i,r}=\lambda_t=2\pi/(mU_0)=100\pi\ . \tag{22}$$

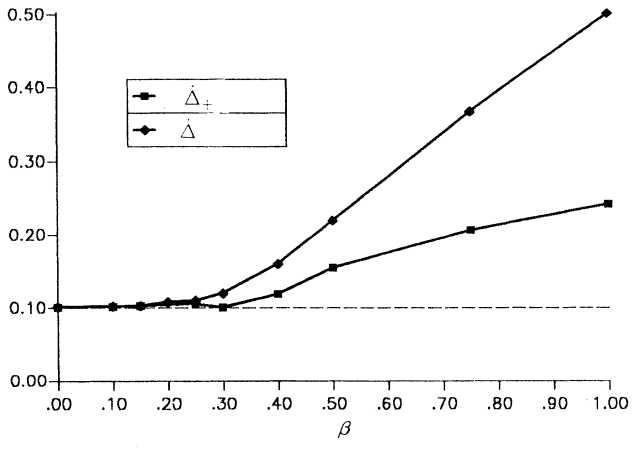

FIG. 3. Time derivative of the mean variance of the hydrodynamic mode (lower curve) and total wave function (upper curve), respectively, as a function of β_0. The mass is set at $m=0.1$, and the initial spreads is $\Delta_0=50$.

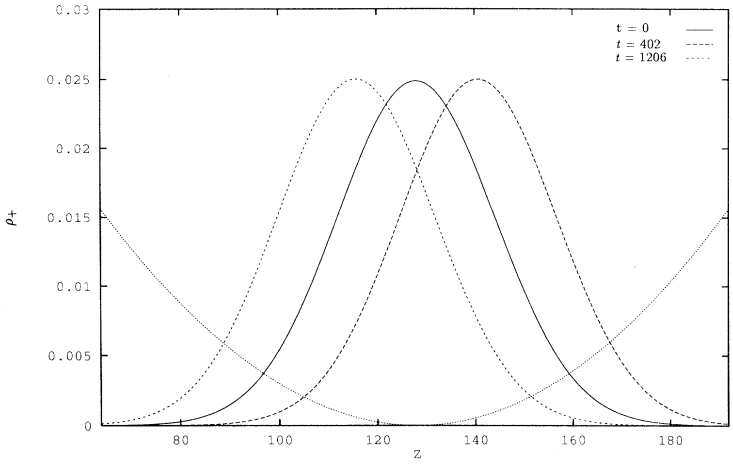

FIG. 4. Localized wave packet bouncing coherently within the harmonic potential. The three profiles correspond to the initial condition (middle), one quarter period (right), and three-quarters of a period (left). The main parameters are $m=0.5$, $V_0=\frac{1}{16}$, $U=0.05$, $L=256$, and $\beta=0.05$.

From this sequence of wave functions, the bounce-back of the wave function as well as its exponentially decaying penetrations into the classically forbidden region is well apparent. In the early stage of the collision, the wave packet slows down abruptly, with a typical profile steepening due to incoming waves piling up over the ones just on the verge of reversing their motion. This gives rise to fast reflected waves with a typical wave number $k\sim mU_0$. As time goes on, these ripples smear out in response to the need of the wave form to regain a smooth backward-propagating Gaussian profile.

Since higher order modes contributing to the initial wave packet never die out, the picture is inherently dynamical in nature and cannot be straightforwardly confronted with analytical steady-state expressions. A typical dynamical feature associated with the presence of these modes is oscillatory behavior also inside the forbidden region. This kind of behavior is clearly detected when the impinging packet is sufficiently narrow so as to contain harmonics whose energy exceeds the potential barrier. This is indeed the case also for the simulation of Fig. 5, in which the fast modes with $k=k_0+2\pi/\Delta_0$ have enough kinetic energy to overcome the potential barrier.

VI. COMPUTATIONAL EFFICIENCY

For a spinless nonrelativistic calculation the QLBE requires two complex words and six complex floating-point operations per grid point. As a comparison, a "classical" one-dimensional Schrödinger scheme would require only half that memory and five complex flops per grid point [5].

This makes a factor 2 less storage and a factor 5/6 (five over six) less computation. Why then bothering about the QLBE? The point is that the above figures do not tell the whole story.

First an explicit Schrödinger solver with a triadagonal spatial stencil (second order derivative) needs two time levels of storage. The QLBE, instead, by involving only one-sided finite differences (upwind first order derivative) can do with one level only; all that is needed is to execute spatial loops in reverse, i.e., cycling against the direction of motion. This closes the factor 2 gap in memory requirements. The factor 5/6 in the computation is a small nuance as compared to other relevant aspects of the time-stepping procedure. A plain explicit Schrödinger solver is known to be conditionally unstable. Several sta-

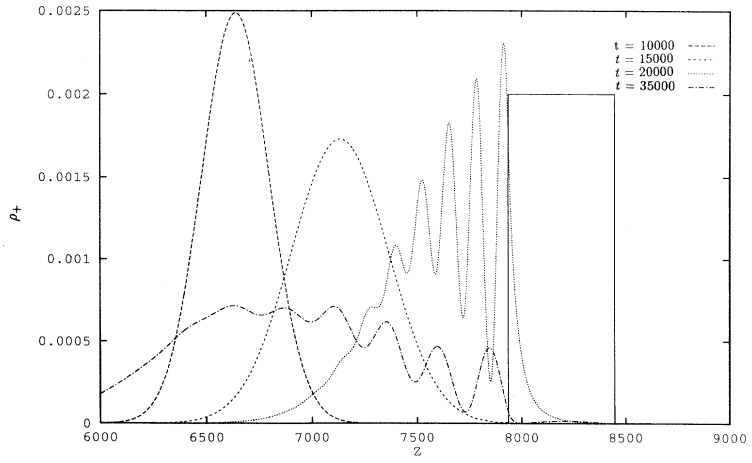

FIG. 5. Localized wave packet impinging against a potential barrier (solid line). The time sequence refers to $t=10\,000$, 15 000, 20 000, and 35 000 time steps. The main parameters are $m=0.2$, $U=0.1$, $V_0=0.002$, $\Delta_0=128$, and $L=16\,384$. The oscillatory behavior of the reflected waves and the exponential decay in the classically forbidden region are clearly visible.

bilization techniques can be devised [6], but none of them—to the best of our knowledge—manages to combine the three features offered by the QLBE: unitarity, dispersion freedom, and unit Courant number (the time step equals the space step in code units).

It is our opinion that his combination is the direct outcome of the hyperbolicty of the Dirac equation as opposed to the parabolic nature of the Schrödinger equation. Artificial hyperbolicity is nothing new in computational fluid dynamics; indeed, the hydrodynamic LBE can be regarded as nothing but a finite-hyperbolicty scheme for the Navier-Stokes equation.

The point is that in the fluid-dynamic context finite hyperbolicity is a mere numerical trick (although one strongly inspired by physical rather than numerical considerations), while in the quantum context the hyperbolic equation bears a fundamental physical meaning: it is the real Dirac equation "in flesh and bones."

The above remarks are not intended to heralding the QLBE as the best finite-difference scheme for the time-dependent Schrödinger equation. Quite the contrary, we believe that, just like in computational fluid dynamics, more accurate—if not more efficient—schemes are definitely available in the modern literature [6,7].

An extensive comparison with the current literature goes way beyond the scope of this paper: on a more qualitative basis we may argue that a point in favor of the QLBE is its ability to secure a number of important features (built-in unitarity, dispersion freedom) while keeping the same computational simplicity of plain explicit schemes.

As to the actual performance, the computer code takes about 1 (μs/step)/grid-point on an IBM RS/6000 mod. 550 superscalar computer workstation, corresponding to about 30 Mflops. This relatively high performance can be traced back to a very efficient execution of complex floating-point operations on the IBM RS/6000 architecture.

By comparison, a simple Cranc-Nicolson scheme, based upon the algebraic Thomas procedure to solve the resulting triagonal system, takes about three times longer on most of the cases examined in this work. The factor 3 reflects the additional operation cost brought about by the Thomas algorithm.

Apart from the serial performance, we are mostly interested in assessing the viability of QLBE on highly parallel architectures. To this end, we first remark that—like most explicit finite-difference schemes—the QLBE is very lean from both computation and communication points of view. Communication is lean because only nearest neighbor connections are involved, and computation is lean because the physics can be lumped into a state-independent 4×4 matrix.

Even counting six flops per complex floating-point operation (actual measurement would yield three) the corresponding communication-to-computation ratio is as low as 4/9 byte/flop. As a result, high parallel speed-ups with QLBE are subject to very stringent requirements on the latency and bandwidth of the parallel machine. This is in a marked contrast with the hydrodynamic LBE which, by featuring several tens of flops per byte, is good for virtually all present-day parallel computers.

Where does this difference stand from? The point is that the hydrodynamic LBE requires many speeds per grid-point and, what is more, the collision matrix acts upon the departures from local equilibria which themselves depend on the local state of the system.

To better focus on this issue, it is convenient to recast the Dirac Eq. (1) into an explicit discrete kinetic-theory format:

$$\partial_t f_i + v_i \partial_z f_i = -ig(f_i - f_i^e) , \tag{23}$$

with the identifications

$$f_i = d,u \ , \quad v_i = \mp 1 \ , \quad i = 1,2 \tag{24}$$

and

$$f_1^e = \frac{i\omega_c}{g} f_2 \ , \quad f_2^e = -\frac{i\omega_c}{g} f_1 \ . \tag{25}$$

This expression highlights the overly simple nature of the local quantum equilibria f_i^e, which are nothing but the distribution function itself times a coefficient. This contrasts with the hydrodynamic LBE, in which local equilibria are quadratic functions of the local speed, which in turn is a linear combination of all discrete populations. The computation of local hydrodynamic equilibria therefore involves a rather computer-intensive task involving of the order of b^2 operations, b being the number of discreet speeds per lattice site. The corresponding QLBE complexity is only $O(2D)$ in D spatial dimensions. This is due to the fact that hydrodynamics is a nonlinearly self-interacting field theory, whereas the quantum equations considered in this work are linear.

The bottom line is that computational advantages such as those we are used to in hydrodynamics, i.e., ease of implementation of complex boundary conditions and outstanding amenability to parallel computing, are likely to surface mostly in situations where nonlinear physics forces a substantial amount of computation into the scattering matrix. The nonlinear Schrödinger equation with local self-interacting potentials *a la* Landau-Ginzburg stands out as a natural candidate for reaping the opportunity of parallel computing.

VII. CONCLUSION

The present results indicate that the quantum LBE is able to reproduce simple nonrelativistic quantum mechanical motion under a variety of physical situations. The resulting numerical scheme exhibits excellent norm-conservation properties, while preserving the swiftness, namely low memory and CPU demand, typical of explicit methods.

Computational efficiency on parallel machines is potentially hampered by low computational density, but is liable to improve significantly once nonlinear interactions are to be dealt with. The viability, both in terms of physical fidelity and parallel computational efficiency, for more complex situations (higher dimensionality and nonlinearly interacting systems) calls for further quantitative investigation.

[1] J. Glimm and Y. Yaffe, *Quantum Physics: A Functional Integral Point of View* (Springer-Verlag, Berlin, 1981).
[2] S. Succi and R. Benzi, Physica D **69**, 327 (1993).
[3] L. Landau and E. Lifshitz, *Relativistic Quantum Field Theory* (Pergamon, Oxford, 1960).
[4] S. Gasiorowicz, *Quantum Physics* (Wiley, New York, 1974).
[5] R. Benzi, S. Succi, and M. Vergassola, Phys. Rep. **222**, 3 (1992).
[6] *Time-dependent Methods for Quantum Mechanics,* Comput. Phys. Commun. Vol. 63, edited by K. C. Kulander (North-Holland, Amsterdam, 1991).
[7] H. De Raedt and K. Michielsen, Comput. Phys. **8**, 600 (1994).